Variations in ENSO Phase Locking*

J. DAVID NEELIN

Department of Atmospheric Sciences and Institute of Geophysics and Planetary Physics, University of California, Los Angeles, Los Angeles, California

FEI-FEI JIN

School of Ocean and Earth Science and Technology, University of Hawaii at Manoa, Honolulu, Hawaii

HSIN-HSIN SYU

Jet Propulsion Laboratory, California Institute of Technology, Pasadena, California

(Manuscript received 7 August 1998, in final form 30 June 1999)

ABSTRACT

A hybrid coupled model (HCM) and a simple coupled model (two variables) for the tropical Pacific ocean–atmosphere system are employed to examine the variations of ENSO phase-locking behavior. The HCM consists of an ocean general circulation model coupled to an empirical atmospheric model. While it is often stated that the warm peak phase of El Niño in observations tends to occur in a preferred season, both model simulations and analysis of observations suggest that the phase-locking behavior is more complicated. A scattered phase-locking behavior in ENSO onset and termination phases is seen in results of both models, even when model climatology is not changing during the integration and weather noise is not included. The mechanisms for this scatter appear to be robust when atmospheric stochastic forcing is included. A similar variation in phase-locking behavior is found in observations, suggesting that the observed scatter of onset and termination phases is a fundamental ENSO property. The scattered phase-locking behavior is explained as a result of a competition between the inherent ENSO frequency (giving a cycle in which warm peaks would not necessarily occur in a preferred season) and the tendency to phase-lock to a preferred season due to the nonlinear interaction between the ENSO cycle and the annual cycle. The phase-locking behavior is associated with the frequency-locking behavior but has additional aspects. For instance, the season of maximum warming can change with parameters, even when the locked ENSO frequency is unchanged. Analysis of observations motivated by the model variation in onset phases suggests defining a category for ''early-onset'' El Niños. Such events appear to be more irregular than other El Niños.

1. Introduction

The El Niño–Southern Oscillation (ENSO) phenomenon is the most prominent interannual oscillation of the tropical climate system. The observed spatial features, temporal evolution, and relationship among oceanic and atmospheric variables are now well known (e.g., Rasmusson and Carpenter 1982; Deser and Wallace 1990; Wallace et al. 1998). ENSO has irregular periods of 2–7 yr, and the warm peaks tend to occur in a preferential season. Considerable theoretical understanding has been gained over the past decades through mechanistic studies with simple and intermediate coupled models (Philander et al. 1984; Anderson and McCreary 1985; Cane and Zebiak 1985; Zebiak and Cane 1987; Battisti and Hirst 1989; Schopf and Suarez 1988; Cane et al. 1990; Wakata and Sarachik 1991; Neelin 1991; Jin and Neelin 1993a,b; Neelin and Jin 1993; Neelin et al. 1994, 1998; Battisti and Sarachik 1995). The oscillatory tendency of ENSO is now fairly well understood, and there are reasonable mechanisms to explain the irregularity of ENSO events, although it is not yet clear which is dominant. The three major contenders as sources of ENSO irregularity are (i) deterministic chaos within the nonlinear dynamics of the slow components of the coupled system (Münnich et al. 1991), particularly, the interaction of ENSO's inherent variability and the earth's seasonal cycle (Jin et al. 1994, 1996; Tziperman et al. 1994, 1995; Chang et al. 1994,

* University of California, Los Angeles, Institute of Geophysics and Planetary Physics Contribution Number 5104.

Corresponding author address: Dr. J. David Neelin, Department of Atmospheric Sciences, University of California, Los Angeles, 405 Hilgard Avenue, Los Angeles, CA 90095.
E-mail: neelin@atmos.ucla.edu

1995); (ii) uncoupled atmospheric weather noise (Kleeman and Power 1994; Penland and Sardeshmukh 1995; Blanke et al. 1997; Eckert and Latif 1997; Kleeman and Moore 1997); and (iii) longer timescale variations affecting the state about which ENSO evolves, for instance, modulation of ENSO by decadal variability. Such decadal variations might originate in the tropical domain (e.g., Latif 1998; Chang et al. 1997) or might be associated with tropical–extratropical interactions via ocean circulations (e.g., Liu et al. 1994; Deser et al. 1996; Gu and Philander 1997). The mechanisms of the tropical–extratropical and ENSO–decadal interactions are not yet fully understood. Of the three, weather noise seems to be the default explanation for a substantial portion of the irregularity.

It is widely stated that the ENSO warm-peak phase is locked to a particular season, namely, boreal winter. Although effects of the seasonal cycle on ENSO are often discussed, the theory for this is as yet not fully developed. A large number of modeling studies suggest that ENSO has an inherent cyclic behavior, and thus preferred inherent periods, when the seasonal cycle is not present. Interaction with the seasonal cycle modifies this inherent cyclic tendency by both linear and nonlinear mechanisms. The linear aspects may be studied with Floquet theory, linearizing a model about a cyclic basic state (Jin et al. 1996). The interannual spatial pattern and evolution is very similar to the case with annual average basic state, but the oscillation is modulated by a seasonal envelope. There is a well-defined interannual period, which is quite well approximated by the annual average case. The interannual ENSO period is independent of the annual cycle in linear results and so is typically not a rational multiple of 1 yr. Thus the interannual cycle tends to produce peak warm phases distributed throughout the year, whose magnitude is modified by the annual modulation. If the annual modulation is very strong, part of the ENSO phasing can be explained by linear mechanisms. However, adjustment of the ENSO period to phase-lock to the annual cycle occurs through nonlinear mechanisms.

Although chaos in the slow parts of the ENSO system may not be the dominant source of ENSO irregularity, the scenario for transition to chaos is very relevant to the modification of the ENSO period and to the phase-locking behavior. The scenario for chaos involves frequency locking of the ENSO cycle to subharmonics of the annual cycle. The nonlinear effects creating frequency locking and phase locking are closely related. These terms are sometimes regarded as synonymous, but for the present study, we find it necessary to make a distinction. Frequency locking occurs when two oscillations with independent frequencies influence one another in such a way as to produce synchronization into a periodic oscillation in which one frequency is a rational fraction of the other. The frequency-locking aspect is studied in the nonlinear dynamics literature (Iooss and Joseph 1990; Bak 1986; Jensen et al. 1984). A typical structure is the ''devil's staircase,'' in which the inherent frequency of the system locks onto a sequence of steps of rational fractions of the external frequency. Overlapping of these frequency-locked steps, caused by increased nonlinearity, leads to chaos due to the erratic jumps between the various overlapping resonance. The phase-locking aspect, on the other hand, is not as well studied, although it is very relevant to ENSO. Here we will use phase locking to refer to the synchronization of the phase (e.g., timing of warming) of the lower-frequency oscillation (e.g., ENSO) with the phase of the higher-frequency oscillation (e.g., the annual cycle). The mechanisms leading to the preferred boreal winter occurrence of ENSO warm phases have been discussed, for instance, by Battisti and Hirst (1989), Xie (1995), and Tziperman et al. (1997, 1998). While the endeavor to understand the phase locking of ENSO to a preferred season is worthwhile, it is also of interest to understand variations of this phase-locking behavior.

The Niño-3 index (averaged SST anomalies over an eastern Pacific area 5°S–5°N, 150°–90°W) from Reynolds SST analysis (Reynolds 1988; Reynolds and Smith 1994) from 1950 to 1998 is displayed in Fig. 1 for 13 El Niño events, aligned based on the year of the maximum warm anomaly. The composite of the 13 El Niño events is represented by the thick light-gray curve. For individual El Niño events, most curves have a maximum or local maximum in winter, but some events have a peak or local maximum in fall or even in the spring months. For example, the 1972/73 El Niño has a peak in December and also a local maximum in August; the 1986/87 El Niño has a peak in September but also a broad warm phase evolving throughout the entire spring season since the winter of the previous year. Although the average shows a peak in the winter months (November–December), the warm phase is actually quite broad, covering the latter half of the year from September to January, and even more so if the 1997/98 event is omitted (figure not shown). Scattered behavior is also found in the phases before (onset) and after (termination) the warm El Niño peaks, for instance, the large variation in amplitudes around October–December prior to the El Niño year [year (−1)] and around May–July in the year after the El Niño year [year (+1)]. We will use ''warm phase'' to refer to the time intervals where anomalies are relatively close to their maximum within a 3-yr interval. Onset and termination here are used with respect to the average cycle and refer to time intervals where the anomalies are small, just prior to, or after, warming. This differs from the Rasmusson and Carpenter (1982) usage of ''onset phase'' and is more like the ''transition phase'' of Latif et al. (1993).

The observational results presented above indicate that there are variations not only in ENSO amplitudes and intervals between warm peak phases, but also in onset and termination phases of El Niños. The widely believed statement that ENSO warm peaks are sharply locked to a preferential season is oversimplified. In this

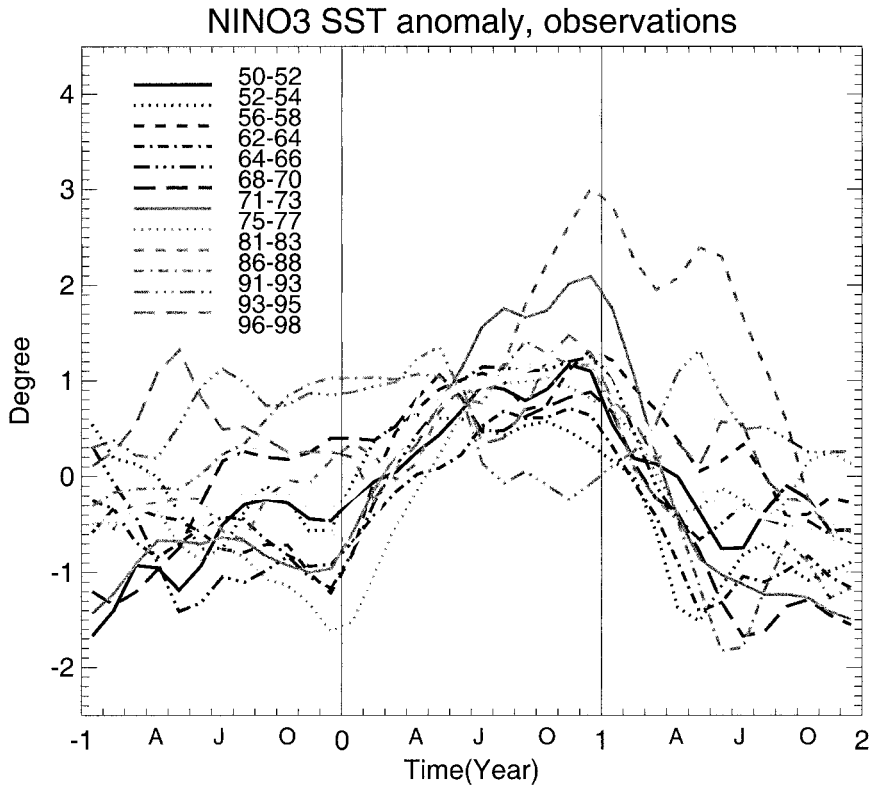

FIG. 1. Niño-3 indices of SST anomaly for 13 observed El Niño events from 1950 to 1998, with the mean seasonal cycle of this period removed. Curves are aligned based on the year of the peak warm phase. The thick light-gray curve represents the average of these warm events. Warm events are selected according to the criteria that warm amplitudes of 3 consecutive months centered in the month of maximum warming exceeds 0.5°C.

paper, the behavior and dynamics of onset and termination phases are examined.

Using two coupled models with different complexity, we examine the ENSO phase variation behavior. One is a hybrid coupled model (HCM), the same as the one used in Syu and Neelin (2000a,b). The other is a simple model, used in Jin (1996, 1997a), in which parameters can easily be varied to examine the sensitivity of parameters to the phase-locking behavior. This paper is organized as follows. Both the HCM and the simple coupled model are briefly reviewed in section 2. The scatter of El Niño onset and termination phases in model results are examined in section 3. The sensitivity of the dependence of phase locking on parameters is further discussed in section 4. The effect of atmospheric noise on phase-locking behavior is investigated in section 5. While analyzing the observed ENSO behavior, it is found that early-onset El Niño events show distinct characteristics from others. We address this point in section 6. Concluding remarks are given in section 7. The purpose of this paper is to address the ENSO phase-locking problem, which requires the presence of the seasonal cycle. Therefore, unless otherwise mentioned in the text, all coupled experiments described in this paper include a prescribed seasonal cycle in climatological wind stress, heat flux, and ocean model climatology.

2. Models

a. Hybrid coupled model

The HCM used in this study is the same as that used in Syu and Neelin (2000a,b) and is similar to the version in Syu et al. (1995), except for a slight change in calculating the empirical singular value decomposition (SVD) model, the inclusion of the atmospheric timescale, and a surface-layer mixing parameterization. The previous version of the HCM (Syu et al. 1995) has applications also in Waliser et al. (1994) and Blanke et al. (1997). The empirical atmospheric model is estimated from observations using an SVD technique. The model contains the first seven SVD modes of the covariance matrix calculated from the time series of pairs of observed monthly mean Reynolds SST and The Florida State University (FSU) pseudostress (Legler and O'Brien 1984) fields (both anomalies) over a 19-yr period from January 1970 through December 1988. Atmospheric timescale (atmospheric spinup time), which was neglected in the previous version, is parameterized,

albeit crudely, in the current version within coupling procedures.

The ocean general circulation model is a version of the Geophysical Fluid Dynamics Laboratory Modular Ocean Model (R. Pacanowski, K. Dixon, and A. Rosati 1991, personal communication) based on Cox (1984). The ocean domain covers the Pacific basin from 30°S to 50°N and from 130°E to 80°W, with continents. A vertical resolution of 27 levels is used, with 10 levels in the upper 100 m. The vertical mixing scheme applied is a modified version of the Richardson number–dependent Pacanowski and Philander (1981) vertical mixing scheme (Mod-Ri scheme). This scheme was developed by B. Blanke (1993, personal communication) and has been applied in various studies (Syu et al. 1995; Blanke et al. 1997; Syu and Neelin 2000a,b). In addition to the Mod-Ri vertical mixing scheme, an ocean boundary layer (surface-layer mixing) parameterization, as employed in Latif et al. (1994), is also applied in some experiments. The different vertical mixing schemes, that is, with or without the inclusion of surface-layer parameterization, significantly affect ENSO periods. Without the surface-layer parametrization, the ENSO cycles lock to a sequence of 2- and 3-yr cycles. When the surface-layer parameterization is included, the ENSO cycles mostly lock to a 3-yr period.

The atmospheric timescale is ignored in our SVD empirical atmospheric model. To account for this factor, which represents important processes in the tropical Pacific area, we represent the atmospheric spinup time (the adjustment timescale for the atmosphere to respond through dynamical processes to changes of boundary forcings) by parameterizing the wind field coupled to the weighted averages of SST anomalies as exponentially decaying with lag time from present at each coupling step:

$$T'_{\text{adj}} = \frac{1}{\eta}\int_0^t T'(t - s)e^{-s/\eta}\, ds, \tag{2.1}$$

where T'_{adj} is the weighted-average SST anomaly (representing adjustment processes) at each time step and η is the averaging timescale. This procedure and an analysis of its impact are examined in the appendix.

In addition to parameterizing the important physics in the tropical atmosphere, we use the atmospheric timescale as a control parameter to examine behavior in regimes with frequency locked to different periods. By changing the spinup timescale, we are able to alter the inherent ENSO periods—that is, in the absence of the seasonal cycle—and the frequency-locking behavior of simulated ENSO cycles when the seasonal cycle is present. Three spinup timescales, 30, 60, and 90 days, are selected to demonstrate the impact on ENSO periods given by the atmospheric timescale. Without the surface-layer parameterization, most ENSO frequencies lock to 2 and 3 yr, while with the surface-layer parameterization, 3- and 4-yr frequency-locking behavior is found.

Based on 30-yr runs, the averaged ENSO periods are calculated (omitting the first cycle). Without the surface-layer parameterization, the average ENSO periods are 2.5, 2.85, 3, and 3.25 yr, with 30-, 60-, and 90-day spinup timescales, respectively. With the surface-layer parameterization, the average ENSO periods are 3, 3.13, 3.57, and 4 yr, respectively. We define the standard version of the HCM as one that includes the surface-layer parameterization and with the atmospheric spinup timescale of 60 days. The standard version of the HCM gives ENSO cycles of 3- and 4-yr periods and reasonable spatial distribution.

b. A simple ENSO model with annual cycle in the basic state

The simple recharge oscillator model of ENSO (Jin 1996, 1997a) is adapted to investigate the variations of ENSO phase locking. From linear dynamics arguments, responses of the equatorial thermocline to anomalous wind stress are determined by the equatorial oceanic dynamic adjustment process. As shown in Jin (1996, 1997a,b), on the ENSO timescale, the eastern and western Pacific thermocline anomalies are approximately described by the following simple adjustment equations:

$$h_E = h_W + \hat{\tau} \tag{2.2}$$

$$\frac{dh_W}{dt} = -rh_W - \alpha\hat{\tau}, \tag{2.3}$$

where h_W denotes the thermocline depth anomaly in the western Pacific, for instance, within one oceanic Rossby radius of deformation from the equator; h_E is the thermocline depth anomaly in the equatorial eastern Pacific; and $\hat{\tau}$ is proportional to the zonally integrated wind stress in this band. The first equation represents the equatorial Sverdrup balance and constrains the east–west contrast of the thermocline depth. The second equation focuses on the thermocline depth changes averaged over the western equatorial Pacific during the basinwide adjustment. The first term on the right-hand side of this equation represents the ocean adjustment. It is characterized by a damping process with a rate r that collectively represents the damping of the upper-ocean system through mixing and the equatorial energy loss to the boundary layer currents at the east and west sides of the ocean basin (Jin 1997b). The wind forcing term $\alpha\hat{\tau}$ is related to the zonally integrated wind stress and its curl. It represents Sverdrup transport across the basin. The zonally integrated effect of this Sverdrup transport will result in slow adjustment of the western Pacific thermocline depth (Wyrtki 1986). The $\alpha\hat{\tau}$ is a weak forcing because only a part of the wind stress forcing is involved in the slow adjustment process, whereas the other part is in the quasi-Sverdrup balance. We will set $\alpha = r/2$ so that at the equilibrium the zonal mean of the equatorial thermocline is zero. These two equations give a gross description of the basinwide

equatorial oceanic adjustment under anomalous wind stress forcing of low frequencies (with timescales larger than the basin-crossing time of oceanic Kelvin waves).

The variation of SST during ENSO is largely confined within the central to eastern equatorial Pacific. The SST anomaly in this region strongly depends on the local thermocline depth that determines the temperature of the subsurface water. This subsurface water is pumped up into the surface layer to control the SST by the upwelling associated with the trade wind along the equator. Changes in the trade wind intensity in response to the SST anomaly may also further reinforce the SST anomaly by altering upwelling and horizontal advection. The mean climatological upwelling and heat exchange between the atmosphere and ocean tend to damp out the SST anomaly. Although the details of all these processes can be complicated (e.g., Zebiak and Cane 1987; Battisti and Hirst 1989; Jin and Neelin 1993a,b), they can be roughly depicted in a simple equation for the SST anomaly T_E, averaged over the central to eastern equatorial Pacific:

$$\frac{dT_E}{dt} = -\varepsilon_T T_E - \frac{\overline{W} + W}{H}(T_E - T_{\text{sub}}) - \frac{W}{H}(\overline{T}_E - \overline{T}_{\text{sub}}), \tag{2.4}$$

where

$$\overline{T}_{\text{sub}} = F(\overline{h}_E),$$
$$T_{\text{sub}} = F(\overline{h}_E + h_E) - F(\overline{h}_E),$$
$$W = \delta_s \tau_E. \tag{2.5}$$

Here, $\varepsilon_T = (150 \text{ days})^{-1}$, $H = 50$ m, and F is a simple function of its argument,

$$F(h) = T_{r0} + \Delta T\left\{1 - \tanh\left[\frac{(h + h_0)}{H^*}\right]\right\}\Big/2,$$

where $T_{r0} = 18°\text{C}$, $\Delta T = 12°\text{C}$, $h_0 = 25$ m, and $H^* = 50$ m. The first term on the right-hand side of Eq. (2.4) is the relaxation of the SST anomaly toward climatology (or zero anomaly) caused by thermal damping processes. The second and third terms are the thermocline and upwelling feedback processes. Anomalous upwelling is approximately related to the local wind stress anomaly τ_E.

Following the discussion in Jin (1997a), the atmospheric wind response to a SST anomaly of the central to eastern Pacific can be simply described as

$$\hat{\tau} = \mu b_0 T_{E_{\text{adj}}}, \qquad \tau_E = \mu a_0 T_{E_{\text{adj}}}, \tag{2.6}$$

where $T_{E_{\text{adj}}}$ takes into account the atmospheric adjustment time at (2.1), as in the HCM; $a_0 = 0.15$ m s^{-1} °C^{-1}; and $b_0 = 15$ m °C^{-1}. Combining the equations and linearizing the coupled system with a realistic and steady basic state, this system supports a coupled oscillatory mode for a wide range of relative coupling coefficients μ as shown in Jin (1997a).

To take the annual variation in the basic state into consideration, we include a simple annual cycle in $\overline{W}$ and $\overline{T}_E$:

$$\overline{T}_E = \overline{T}_{E_0} + \Delta_T \sin(\omega t),$$
$$\overline{h}_E = -0.4 b_0 (30°\text{C} - \overline{T}_{E_0}),$$
$$\overline{W}_0 = -a_0(\overline{T}_E - 30°\text{C}), \tag{2.7}$$

where $\overline{T}_{E_0} = 25°\text{C}$, $\Delta_T = 2.5°\text{C}$, but neglect the small annual variation in $\overline{T}_{\text{sub}}$. Equations (2.2)–(2.7) form a simple anomaly coupled system with a prescribed annual cycle basic state. In its annual basic state, cold tongue temperature reaches its highest temperature in April ($\omega t = \pi/2$) when upwelling is also the weakest. These features in the simple annual cycle are roughly in agreement with those of the annual cycle in the HCM. Thus this simple coupled model shares a similar basic state and a similar anomaly coupling strategy as that employed in the HCM. Comparison of the oscillation mechanism in Syu et al. (1995) and Syu and Neelin (2000a) with that in Jin (1997a,b) suggests the simple model is a plausible analog for the dynamics in the HCM, although we note the caveat that this has not been conclusively proven. Even if the simple model dynamics should prove to be an imperfect representation of the more complex ENSO behavior, the frequency-locking and phase-locking behavior can still be a useful analog for understanding this aspect in the HCM.

3. The scatter of El Niño onset and termination phases

a. HCM results

The Niño-3 index of 13 model-simulated warm events for the standard case with the HCM is shown in Fig. 2a. Although the simulated El Niños have more regular behavior and smaller variations in the amplitude of the peak warm phases than they do in the observations, there are still large variations in the onset and termination phases. This point is further illustrated by Fig. 2b. The black curve represents the average of the 13 warm events, and the gray vertical bars represent plus and minus one standard deviation of the 13 events for each month. During both onset and termination phases, the standard deviation is large, representing more scattered behavior, while a more consistent phase-locking behavior is found in the warm-peak phase (small standard deviation). The climatology of the coupled simulation is not changing during integrations. In addition, no atmospheric noise is added in the model, and the wind anomaly field only reacts to low-frequency SST variations through the SVD atmospheric model. However, even under such ''perfect'' conditions, the model results show scattered phase-locking behavior in onset and termination phases.

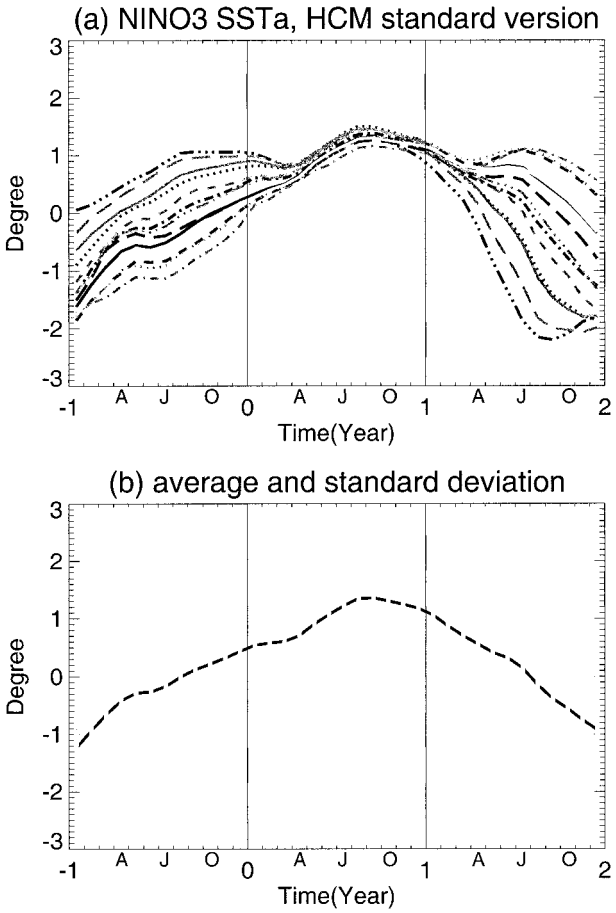

FIG. 2. (a) As in Fig. 1, but for the hybrid coupled model results with the standard version. Thirteen consecutive model El Niño events from a total 153-yr simulation are included here. (b) Mean (black curve) and standard deviation (vertical bars) of the 13 events shown in (a). Warm events for this case and all model results in the paper are selected according to the criteria that maximum warm amplitude exceeds the standard deviation of the whole time series.

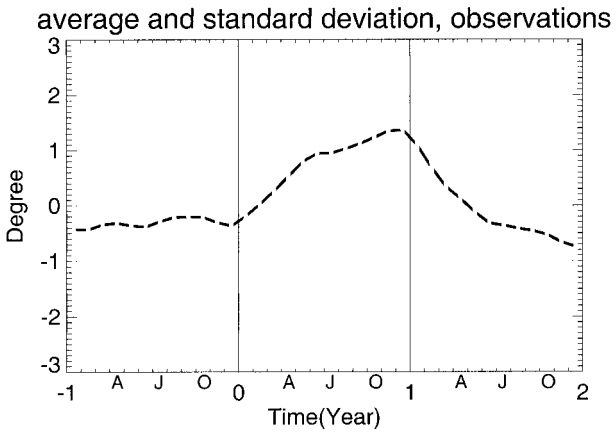

FIG. 3. As in Fig. 2b, but for the observations in Fig. 1.

The variation of ENSO phase found in observations (Fig. 1) is further illustrated in Fig. 3. Similar to Fig. 2b, the average (black curve) and standard deviation (vertical bars) of the 13 events from observations are shown. Larger than normal standard deviation is seen in the warm-peak phase, onset phase, and termination phase. Although the observed El Niño events have more variability in the warm-peak phases, the magnitudes and features of the large standard deviation in onset and termination phases are similar to the model results. From the analysis above, the observed warm El Niño phases are not sharply locked to a particular season. Rather, the warm El Niño events have scattered warm peaks, broadly covering the second half of a year, while the onset and termination phases show variations of comparable standard deviation. If the 1997/98 event is omitted, the onset and termination phases actually have larger standard deviation than occurs during the warm phase (figure not shown). The similarity of the scattered phase-locking behavior in onset and termination phases between the observations (Fig. 3) and model results (Fig. 2b) suggests that the scattered phase-locking behavior may be an intrinsic phenomenon in the ocean–atmosphere coupled system. It must be borne in mind that atmospheric stochastic forcing or secular changes leading to exceptional events are also potential explanations of variation among ENSO events, but the model dynamics suggests a deterministic mechanism may contribute.

Several types of phase-locking behavior are shown in the model warm events associated with different vertical mixing schemes and atmospheric spinup timescales. However, the effect of these physical parameterizations to the ENSO phase-locking behavior occurs mainly via the change of ENSO period and frequency-locking behavior. As mentioned in section 2a, with different vertical mixing schemes and spinup timescales, the averaged ENSO periods are changed, while the phase-locking behavior is also different as illustrated in Figs. 4a–f.

The first type of phase-locking behavior, as shown in Figs. 4c and 4f, has all El Niño events phase locked to the same season (single phase-locking type). For this type, only one frequency, locked to integer years, exists in the simulated ENSO cycles, for example, 4 yr in Fig. 4c and 3 yr in Fig. 4f. The second type of phase-locking behavior, represented by the case in Fig. 4d, consists of two or more groups of phase-locking behavior (multiple phase-locking type). For example, there are two groups in Fig. 4d, and each group has its own preferential peak phase: one is from May to June and the other one around September. The frequency-locking behavior for this case shows a repeated sequence locked to 2- and 3-yr periods [Fig. 5a, after Fig. 11a in Syu and Neelin (2000a)]. The 2-yr frequency-locking events tend to phase-lock to earlier months than do the 3-yr frequency-locking events.

The third phase-locking type, the most common type,

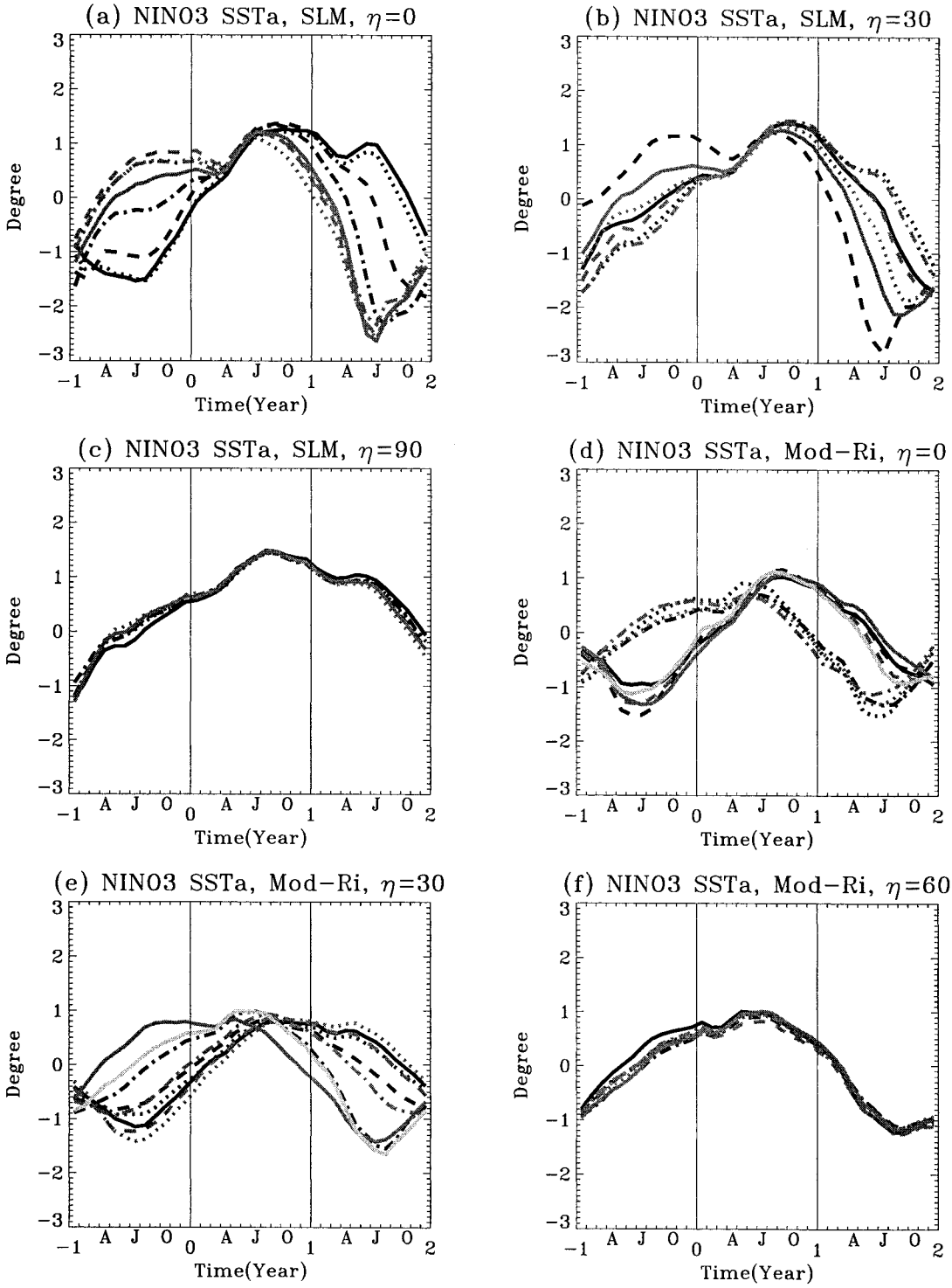

FIG. 4. Niño-3 indices of SST anomaly for 30-yr model simulations with the surface-layer parameterization and with various values of the atmospheric spinup time: (a) $\eta = 0$ (inherent period 3 yr), (b) $\eta = 30$ days (inherent period 3.35 yr), (c) $\eta = 90$ days (inherent period 4.05 yr); and without the surface-layer parameterization and with atmospheric spinup time: (d) $\eta = 0$ (inherent period 2.5 yr), (e) $\eta = 30$ days (inherent period 2.8 yr), and (f) $\eta = 60$ days (inherent period 3.1 yr). Anomalies for each case are with respect to its own mean seasonal cycle. The number of warm events included are, respectively, 8, 7, 6, 9, 9, and 8.

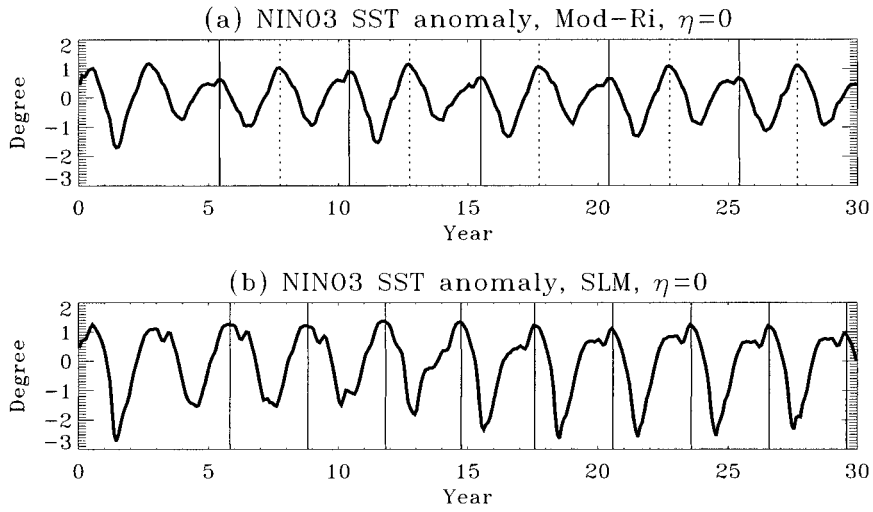

FIG. 5. Niño-3 time series of SST anomaly (a) for the case in Fig. 4d, (b) for the case in Fig. 4a; (a) and (b) are after Figs. 11a and 10a in Syu and Neelin (2000a), respectively. Thin solid vertical lines represent 3-yr period cycles, counting from the previous warm peak. The dotted vertical lines represent 2-yr period cycles.

represented by the cases in Figs. 4a, 4b, and 4e, shows scattered phase-locking behavior (scattered phase-locking type). There is a tendency for this type of cycle to share the same peak phase to a greater (Fig. 4b) or lesser (Fig. 4e) extent. For example, the case in Fig. 4a has three groups of El Niño events showing different phase-locking behavior. One group tends to show a broad warm phase from July of the year before the El Niño year [year (−1)] to January of the El Niño year [year (0)], and a warm peak around August, year (0). Another group has a broad warm peak from August to December, year (0), and a second warm peak around June of the year after the El Niño year [year (+1)]. The third group shows only one dominant peak around August of the El Niño year (e.g., the dark dashed line). From the Niño-3 time series for this particular case (Fig. 5b, after Fig. 10a in Syu and Neelin (2000a)], a relationship between the phase-locking behavior and individual ENSO cycles can be examined. It is found that the first three cycles show a broad warm peak at year (0) and a secondary one in year (+1). The last 3–4 cycles have a feature of broad warm phase in year (−1) and a warm peak in the El Niño year. The cycles containing only one warm peak, occurring between the other two groups of cycles, seem to be transitional events. This case has intervals between warm events mostly locked to 3 yr (except for the first cycle), but with the locking occurring in slightly different patterns in different years.

We note that the analysis method of aligning cycles indexed on the warm phase is based on the fact that ENSO warm peaks tend to be phase locked (Rasmusson and Carpenter 1982; Horel 1982; Deser and Wallace 1990). When tested on finite-length runs with no annual cycle, some artifacts were noted, so the method is only appropriate if phase locking is sufficiently strong.

b. Simple-model results

The simple model, with drastic reductions in degrees of freedom, appears capable of describing the essential impact of the annual cycle on the ENSO. It basically reproduces the main phase-locking characteristics found in the HCM. A typical solution of the simple model is shown in Figs. 6a and 6b. This is a nearly periodic solution whose frequency is closely approximated by a rational frequency m/n such that $m < n$. In this particular solution, $m = 17$, $n = 58$. In other words, every 58 yr, there are about 17 model ENSO events. Although there is some variation in warm phases, they are very narrowly confined in the summer season. Similar features are evident in Figs. 6c and 6d for a solution in a very different parameter regime. In the latter case, the Ekman feedback is much reduced and the warm phases tend to be more phase locked to a winter season with greater spread. Clearly, the phase locking of El Niños is sensitive to the changes in parameter regimes, which will be further addressed in section 4. Moreover, in both cases, similar to the HCM results, there is much greater phase scatter during onset and termination phases of ENSO warming.

4. Sensitivity of phase locking

a. HCM results

With the surface-layer parameterization, most cases phase-lock with the warm phase in the fall season,

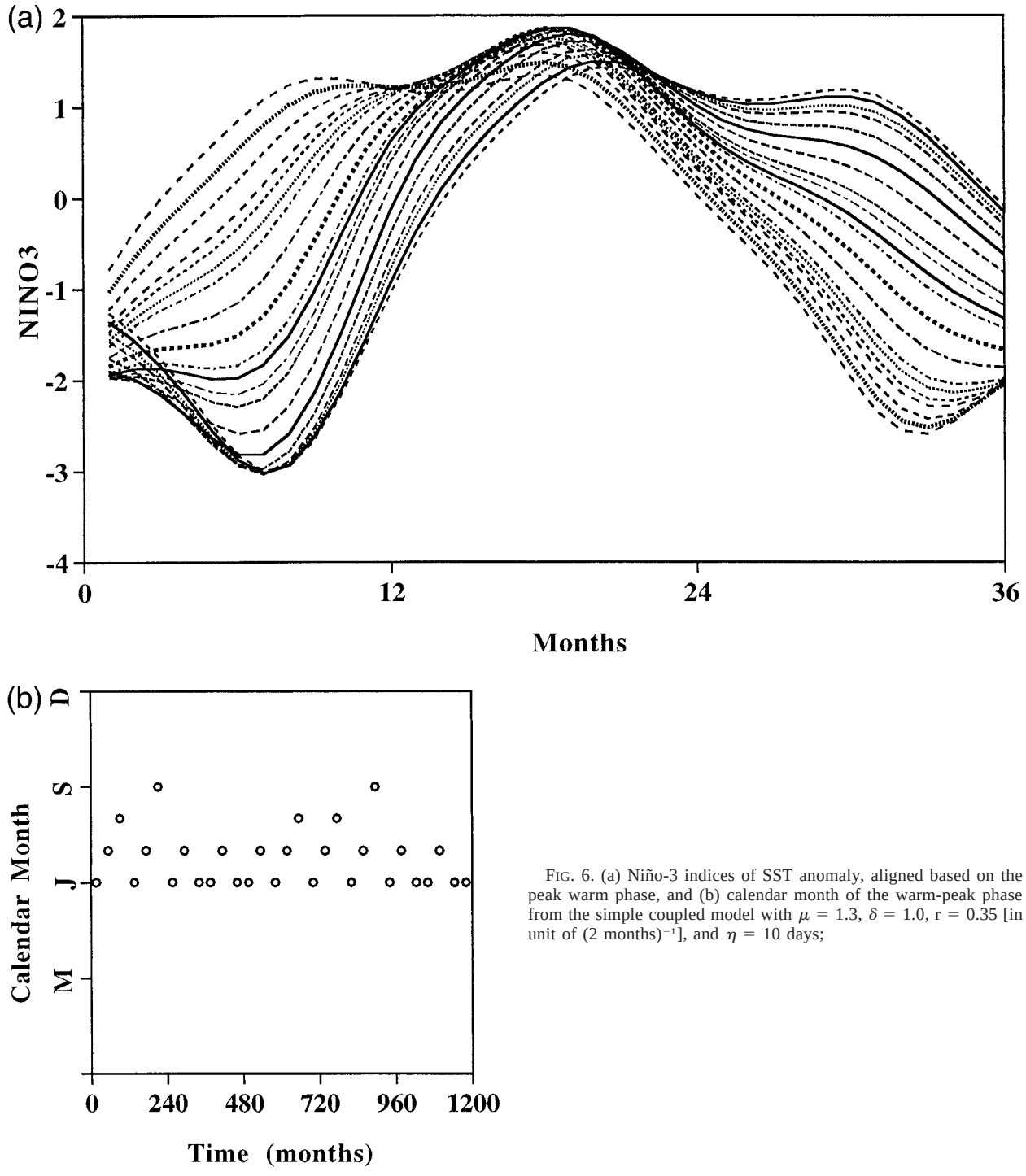

FIG. 6. (a) Niño-3 indices of SST anomaly, aligned based on the peak warm phase, and (b) calendar month of the warm-peak phase from the simple coupled model with $\mu = 1.3$, $\delta = 1.0$, r = 0.35 [in unit of (2 months)$^{-1}$], and $\eta = 10$ days;

that is, August–September (Figs. 4a–c). Without the surface-layer parameterization, the phase-locking behavior is a little more complicated, but with a tendency to lock to June–August (Figs. 4d–f). The changes of phase-locking behavior shown in the examples in the previous section are related to the changes of frequency-locking behavior, which is briefly reviewed in section 3a. However, an exception was found with different phase-locking behavior for the same frequency-locked ENSO periods. This occurs for one case when very small changes are made to the atmospheric model. The case without the surface-layer parameterization and with the atmospheric spinup time of 60 days in the current model exhibits a pre-

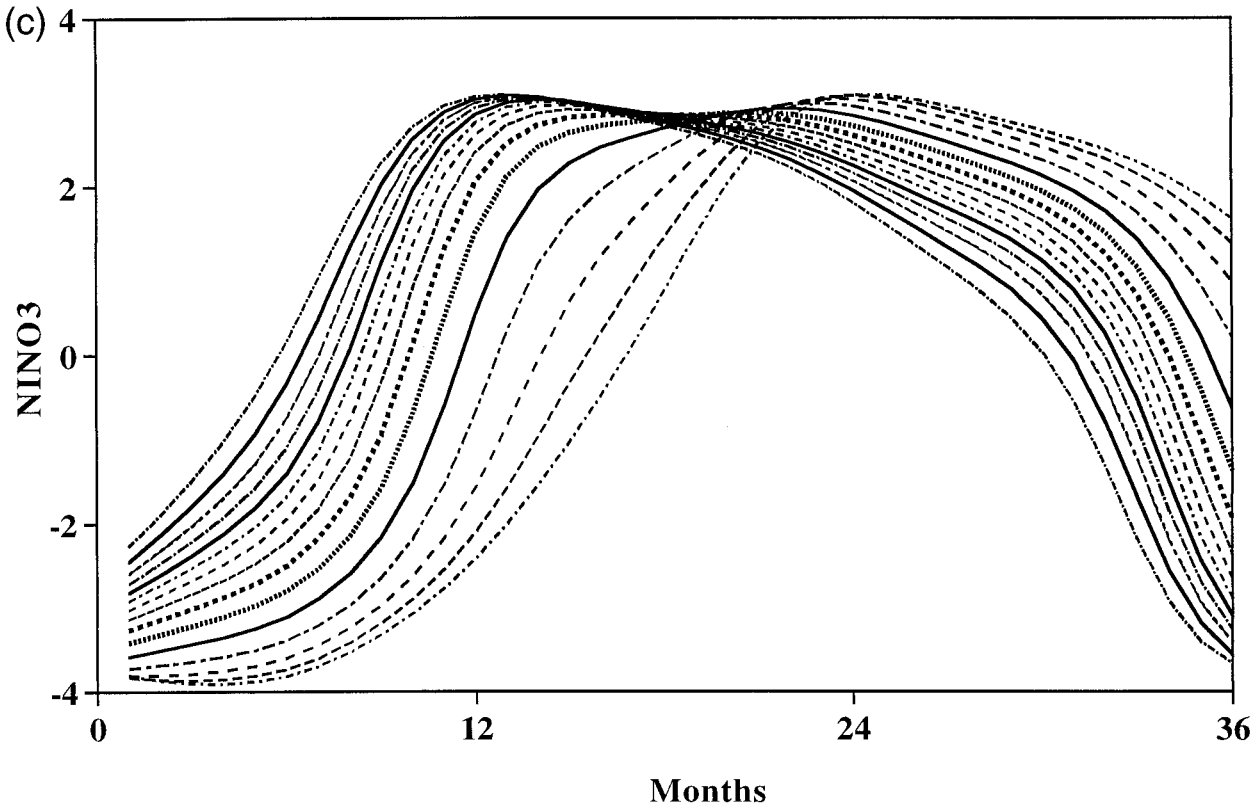

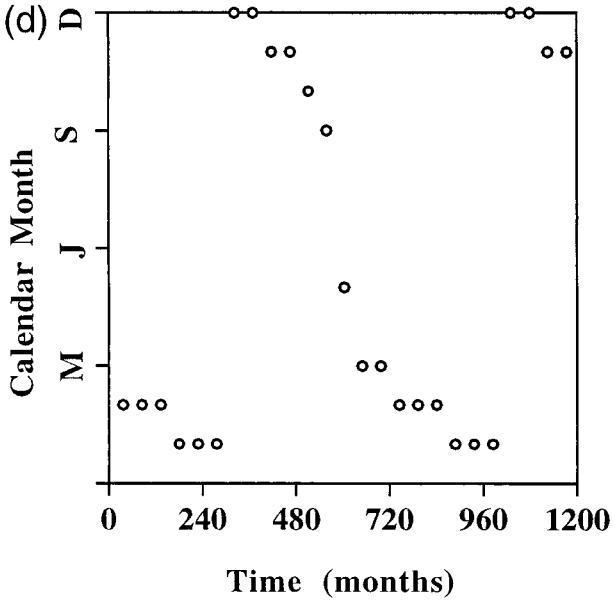

FIG. 6. *(Continued)* (c) and (d) are as in (a) and (b), but for a case with different parameters $\mu = 1.3$, $\delta_s = \frac{1}{3}$, r = 0.25, and $\eta = 0$.

ferred June–August peak warm phase (Fig. 4f). A small change in the atmospheric model, however, is found to affect this. Using the SVD model as estimated in Syu et al. (1995), which differs only in details, the results of Fig. 7 are obtained. The preferred season for the peak warm phase has shifted to January. It is possible that slightly changed parameters can affect the frequency-locking behavior, thus changing the phase-locking behavior. However, this explanation does not apply to the cases discussed here, because both cases demonstrate a same 3-yr frequency-locking behavior. The surprisingly sensitivity of the phase locking is explained below in terms of the simple model.

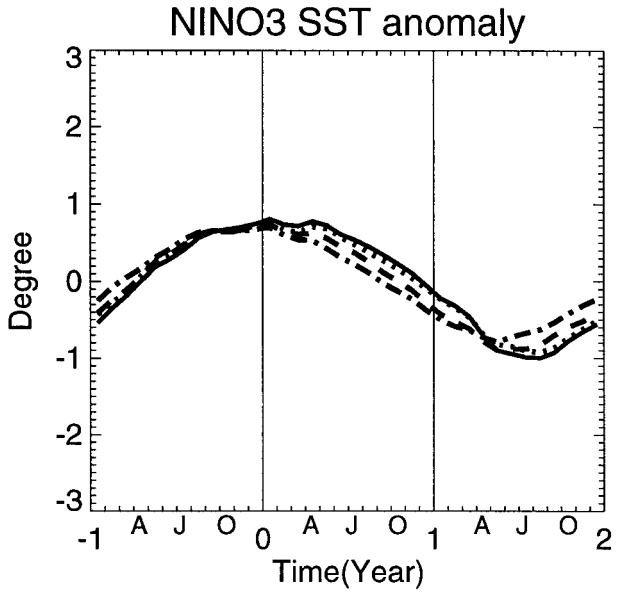

FIG. 7. As in Fig. 4f, but with a slightly different SVD atmospheric model as used in Syu et al. (1995). Four warm events are included in this case.

b. Simple-model results

The simple model features the devil's-staircase-type frequency locking of ENSO under the annual cycle forcing as was first illustrated by Jin et al. (1994, 1996) and Tziperman et al. (1994). Here we only focus on two particular frequency steps of the devil's staircase with frequency-locked solutions of 3- and 4-yr periods, respectively. On each step, the coupling coefficient varies in a rather narrow range and the period stays the same. However, there is a continuous shift of the peak warm phases in the solutions on the same step for different coupling coefficients as shown in Figs. 8a–d. For the solutions on the 3-yr step, the range is from July to January (Figs. 8a,b). For the solutions on the 4-yr step, the phases of the absolute maxima of SST for the ENSO warming events change from February to November (Figs. 8c,d). We note that the apparent jump in phase in Fig. 8c is merely due to the flattening of the peak during maximum warming. The overall behavior changes smoothly with the coupling coefficient. The significant yet continuous shifts in the phases of frequency-locked solutions of same period within a very narrow range of coupling coefficient provide a prototype model for the different solutions shown in Figs. 4f and 7 from the HCM.

Some of the effects producing these continuous shifts in phase are as follows. The coupled inherent periods are not an integer number of years, but the intervals between two warm peaks are forced to lock to an integer year by the interplay of the nonlinearity with the seasonal cycle. The timing of the warm phases is adjusted by the nonlinearity trying to match the preferred season. For instance, if the inherent period is slightly longer than 3 yr, the warm phase is forced to occur earlier than it otherwise would to match the preferred season every third year. When a parameter is varied, it affects the degree of nonlinearity and the inherent period and, hence, affects the balance between these effects, resulting in a shift in the season of warming. For instance, consider a case where the inherent period would tend to increase with the parameter if the seasonal cycle were absent. In presence of the seasonal cycle, the ENSO cycle can be held to 3 yr by the nonlinear interactions. In this case, one would expect a tendency to shift the timing of the peak later in the cycle. The case shown, however, is more complicated, since the inherent period changes only from 35 to 37 months in the range of coupling values on the 3-yr locked step. The amplitude changes by roughly 15% in this range, suggesting that changes in the nonlinear effects are actually more important. This points to a complex mechanism setting the timing of the warm phase; even for a given climatological seasonal cycle, subtle changes in parameters can affect the timing.

In the simple model, one can loosely divide the phase-locking behavior into two scenarios: the strongly phase-locked and weakly phase-locked scenarios. In the strongly phase-locked regime, the warm phases stay almost unchanged either in a solution for a fixed parameter or in solutions for different parameters. An example of this type of solution is shown in Fig. 9a. In this case, every 7 yr there are two warm events, but the peak warm phases stay around June to July. To make this possible, the intervals between warm events alternate between 3 and 4 yr. In other words, due to phase locking to the annual cycle, the intervals between events of ENSO are forced to adjust to integer numbers of years. In the weakly phase-locked regime, however, the seasonal timing of the peak warm phases changes in a solution for a fixed parameter or in solutions for different parameters. A striking example of this type of solution is shown in Fig. 9b. In this case, every 7 yr there are also two warm events. But the peak warm phases now occur in March and October, alternately. The interval between warm events stays almost constant, alternating between 41 and 43 months. In this case, phase locking of ENSO to the annual cycle does not greatly alter the periodicity of the ENSO mode but leads to multiple warm phases. Similarly, the HCM case in Fig. 4d has 28- and 32-month intervals alternating. Another example of this type of weakly phase-locked solution is given in Figs. 9c,d, where the solutions have four different phases. There are four El Niños every 13 yr, with intervals between warm peaks of 41, 39, 38, and 38 months, respectively. Although the two types of phase-locking scenarios are different, they share a common feature, that is, the great phase scatters during both onset and termination phases of ENSO warming as shown in section 3. We caution that the HCM behavior does not always fall neatly into these two categories, as seen in section 3a.

5. Effect of noise on phase locking

The atmospheric weather noise can be important, including as a source of ENSO irregularity (e.g., Zebiak 1989; Penland and Sardeshmukh 1995; Jin et al. 1996; Chang et al. 1996; Blanke et al. 1997; Eckert and Latif 1997). Several studies have also investigated the effect of atmospheric noise on ENSO phase-locking behavior. Jin et al. (1996), Chang et al. (1996), and Blanke et al. (1997) found the preferred season for the warm phase to be similar with and without weather noise. They concluded that the phase locking is associated with the frequency-locking behavior and that the addition of atmospheric noise does not strongly alter this property. These studies focus on the statistical behavior of El Niño peak phases rather than variations in onset and termination phases. The HCM exhibits interesting variations in phase-locking behavior even without the inclusion of atmospheric noise: with some parameters, the HCM strongly locks to a single, integer-year period, and little variation is found in onset and termination phases; with other parameters, the HCM locks to a succession of different integer-year intervals, and large variations in onset and termination phases are found. To test the robustness of the mechanisms for phase-locking behavior, we include noise forcing in the HCM. The impact on ENSO phase, especially in onset and termination phases, is then evaluated.

The estimate of the noise component used here is estimated from observations following Blanke et al. (1997), by a method that retains the spatial structure of the noise fields. The monthly residual wind is computed as the difference of the observed FSU wind anomalies (from January 1970 to December 1988, total 228 records) from the reconstructed wind anomalies from SVD modes that retain only the portion of the stress linearly coupled to the underlying SST anomaly field. This residual wind is sampled randomly in time during the coupled integrations. Noise maps are decorrelated on 1-month timescales but interpolated to a time step of 1 day. The noise product is chosen independent of season for two reasons: (i) the dataset is not long enough to reliably estimate seasonal dependence; (ii) so that it is clear that seasonal effects are entirely within the deterministic part of the system in these results.

a. Effects on onset scatter

Figures 10–12 show the Niño-3 indices of individual El Niño events (Figs. 10a, 11a, 12a) and the mean and standard deviation of the El Niños (Figs. 10b, 11b, 12b) with noise for different cases corresponding to Figs. 2 (scattered phase-locking type), 4c (single phase-locking type), and 4d (multiple phase-locking type), respectively. All cases show more irregular behavior when the noise is included, and larger standard deviation is obtained during the peak warm phase for the case with noise. However, the scattered behavior (i.e., large standard deviation) in onset and termination phases for cases in Figs. 10 and 12 appears to be similar to the cases in Figs. 2 and 4d, in which large variations in onset and termination phases occur even without noise. This implies that the mechanisms that cause the variation of ENSO phases are quite robust—nonlinearity tries to pull inherent phases toward a preferred season, while the inherent period, if not an integer year, tends to move the maximum warming away from the preferred season. The onset phases thus are affected by the accumulated effects from the past.

In a case where there is no trade-off between the tendencies due to the inherent period and the phase locking in setting the timing of maximum warming (e.g., the case in Fig. 4c, with a perfect 4-yr cycle and thus no variations in onset phases without noise), noise appears to simply restore a trade-off between similar mechanisms (Fig. 11) by resetting the phase. That is, without noise, the inherent period arrives at the preferred season, but if noise changes the phase of the oscillation, phase-locking mechanisms tend to stretch or shrink the cycle to match the preferred season.

b. Does noise shift the ENSO peak?

In both Jin et al. (1996) and Blanke et al. (1997), the warm-peak phases are locked to the same preferential seasons in both cases with and without atmospheric noise. We obtain similar results in some cases (e.g., cf. Fig. 4c to Fig. 11 and Fig. 4d to Fig. 12). Some El Niño events in our standard case when the atmospheric noise is included have peak phases shifted from the fall (August–September) season (Fig. 2a) to the winter (November–January) season (Fig. 10a). The averaged peak phase in this case is thus broadened (Fig. 10b), covering from August to December, compared with the case without noise (Fig. 2b). This raises the question of whether noise could have a rectified effect on the peak. While examining whether this behavior is systematic, we found considerable sensitivity to the number of events included in the average. This suggests that taking, say, a 40-yr record, like the observed record, may not be sufficient to define the preferred month with high precision. The results will be subject to random variations due to weather noise.

6. Early-onset El Niños

In an attempt to categorize the observed warm events in terms of the phase-locking behavior, we define an onset index, which is the 3-month mean of the SST anomaly centered 12 months in advance of the average peak month of the 13 observed El Niño events. There are two reasons for choosing 12 months in advance of the averaged peak to define the onset index. First, 12 months is approximately one-quarter of an ENSO cycle, with an average 4-yr period. Second, 12 months ahead

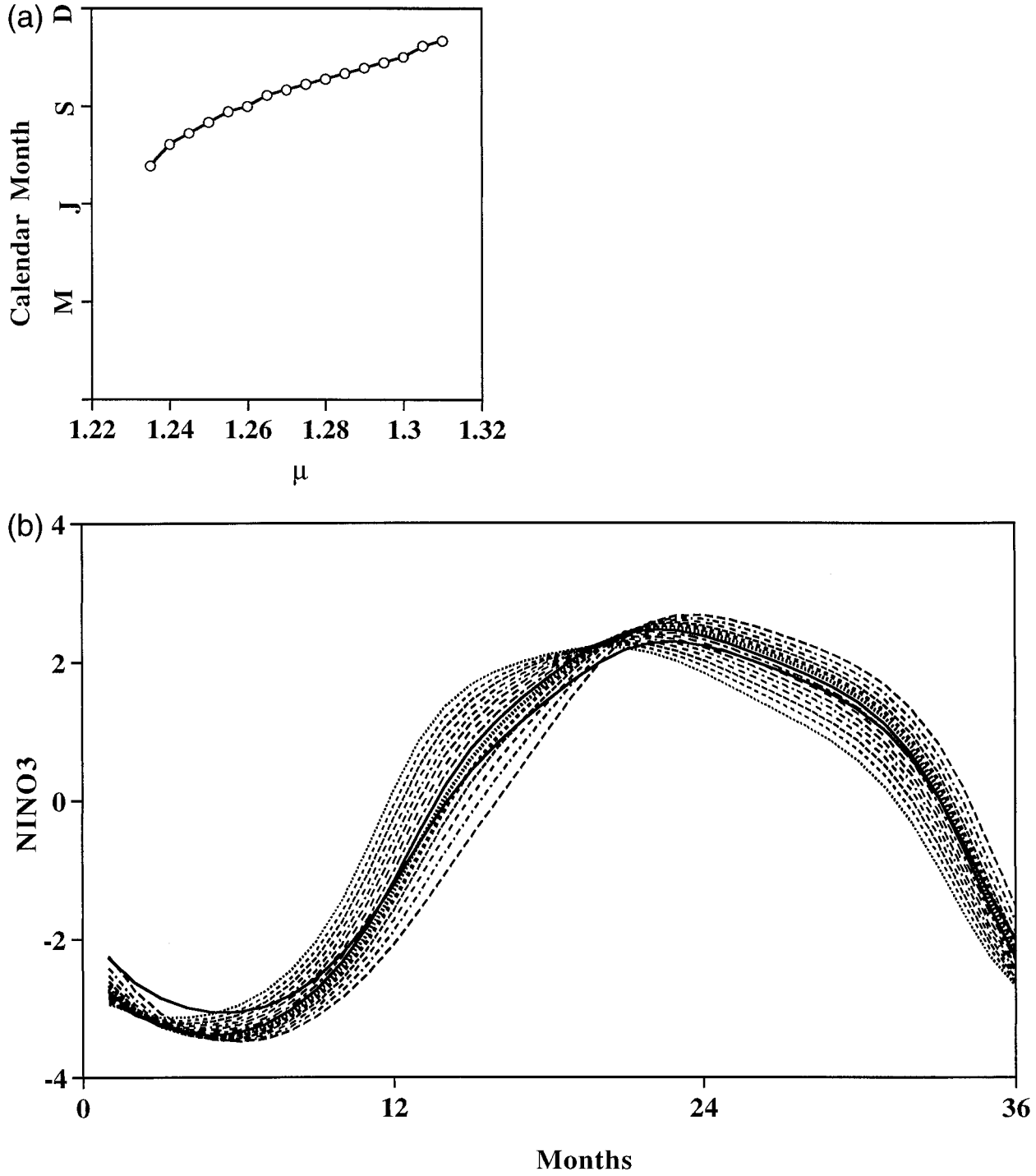

FIG. 8. Dependence of warm phase on the coupling parameter within a single frequency-locked step. (a) Calendar month of the peak warm phase, and (b) Niño-3 indices of SST anomaly aligned based on the peak warm phase of model ENSO cycles with a 3-yr period from the simple coupled model, with $\delta_s = 1/3$, $r = 0.35$, and $\eta = 0$. One warm event is shown for each value of μ in the range $\mu = 1.235$ to 1.315.

of the average peak warm phase corresponds to the maximum standard deviation seen in Fig. 3, within the interval immediately prior to the event.

Any warm event with an onset index larger than the mean onset index (of the total 13 El Niños) is categorized as an ''early-onset'' event. Figure 13 shows both early-onset events (Fig. 13a) and other events (Fig. 13b). The behavior of warm events in both categories shows considerable difference. Most early-onset events have broad and scattered warm phases, while other El Niño

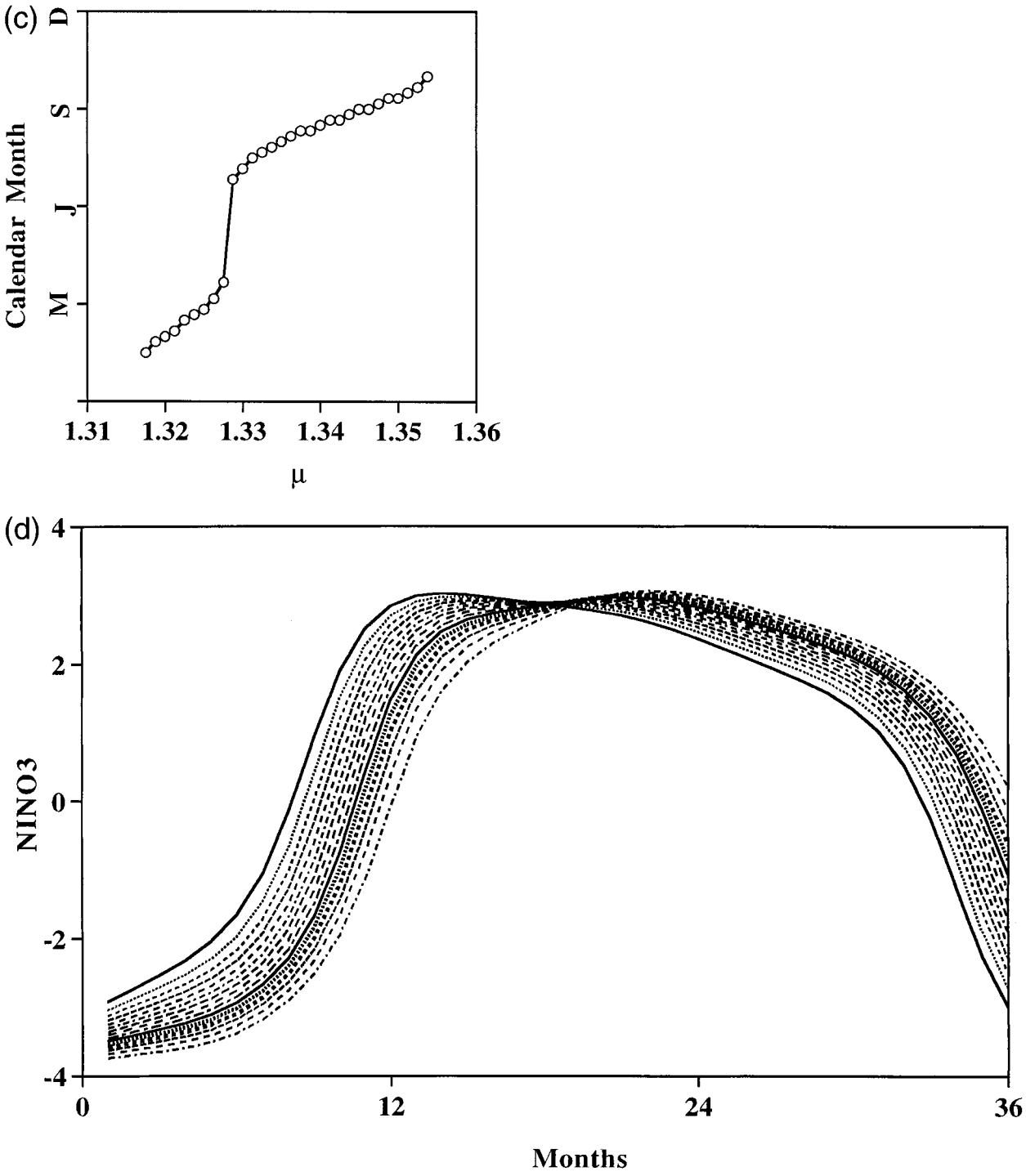

FIG. 8. *(Continued)* (c) and (d) are as in (a) and (b), but for a case with a 4-yr period and with $\mu = 1.3175$ to 1.355, $\delta_s = \frac{1}{3}$, $r = 0.2$, and $\eta = 0$.

events show more regular and consistent behavior among individual cases.

With suitable seasonal phase to start with (onset), there is no tension between evolution due to the inherent period and matching to the preferred season. Therefore, the ENSO warm events that are not early onset (by this definition) show a more consistent behavior in phase development. Judging from the regular behavior, El Niño events that are not early onset might be conjectured to be easier to predict. For early-onset El Niño events,

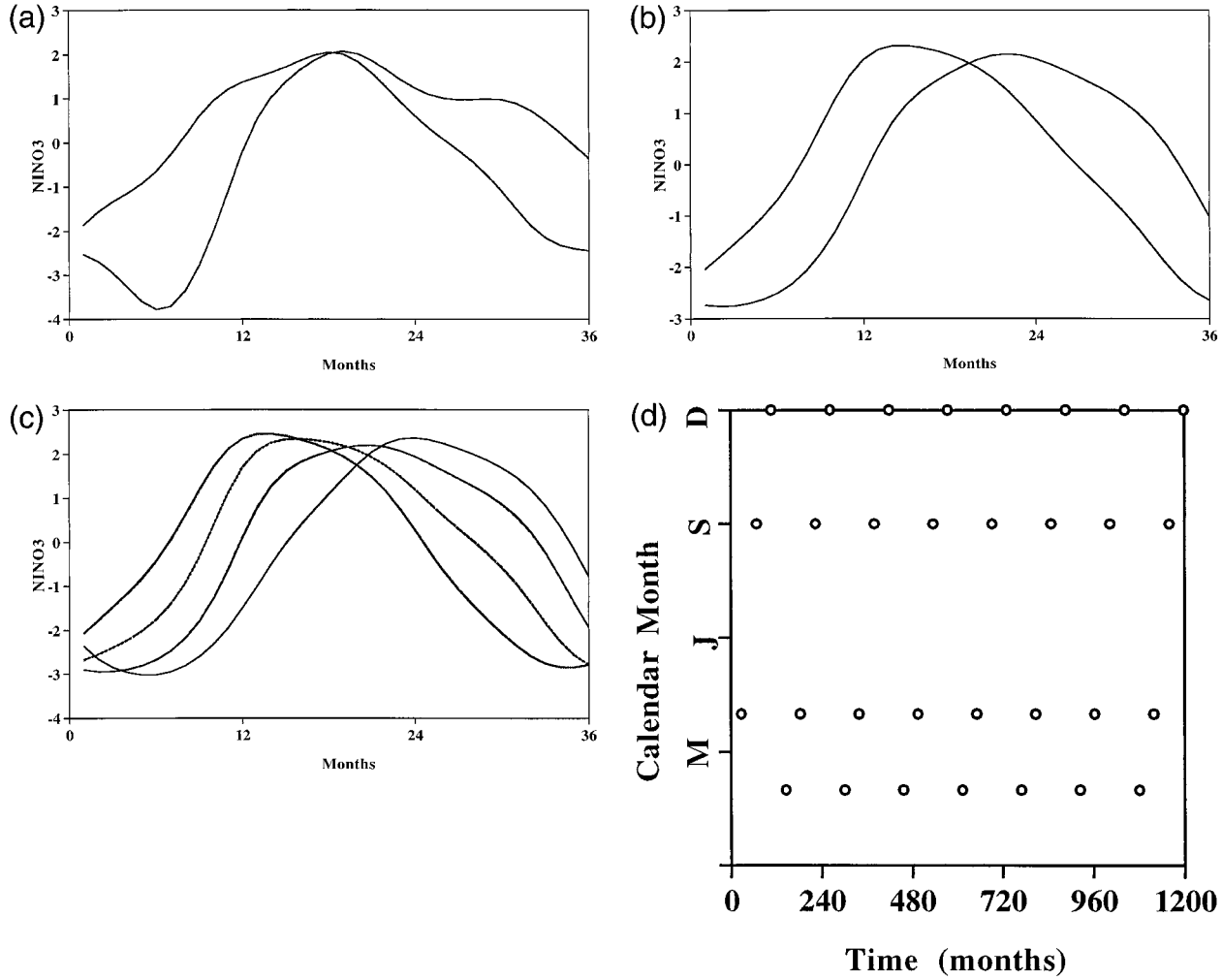

FIG. 9. (a) As in Fig. 6a, but for the case with $\mu = 1.3$, $\delta_s = 1$, $r = 0.35$, and $\eta = 0$; (b) as in (a), but for the case with $\mu = 1.25$, $\delta_s = ⅓$, $r = 0.35$, and $\eta = 22.5$ days; (c) as in (a), but for the case with $\eta = 11.8$ days; (d) calendar month of the warm-peak phase for the case in (c).

nonlinearity tends to act more strongly to force the peak phase toward the preferential season. Since more nonlinearity is involved, we conjecture that the El Niño development thus is less regular. Therefore, early-onset events show more scattered behavior and may be harder to predict. Although the 1997/98 El Niño developed rapidly once it began, it was not an early-onset El Niño event according to our definition and thus falls in the category conjectured to be easier to predict, perhaps contributing to the success of forecasts. Experiments assessing forecast model skill for events stratified according to onset time might be interesting to evaluate.

7. Conclusions

ENSO phase-locking behavior is examined using observations of Niño-3, an HCM, and a simple coupled model. While it is widely believed that the warm-peak phase of El Niño tends to occur in a sharp preferential season, both observations and model simulations suggest that the phase-locking behavior is more complicated. A scattered phase-locking behavior in El Niño onset and termination phases is seen in the standard version as well as many other sensitivity experiments of the HCM, even in regimes that have well-defined frequency locking. The simple coupled model gives consistent results in the variation of phase-locking behavior. Both the HCM and the simple coupled model results show that variation of onset and termination phases can still occur even in a model in which no weather noise is included, model climatology is not changing during integration, and parameters are fixed. Examining the Reynolds SST Niño-3 index, similar scattered phase-locking behavior is found. Large deviations exist in observed El Niño onset and termination phases as well as in the amplitude of warm-peak phases.

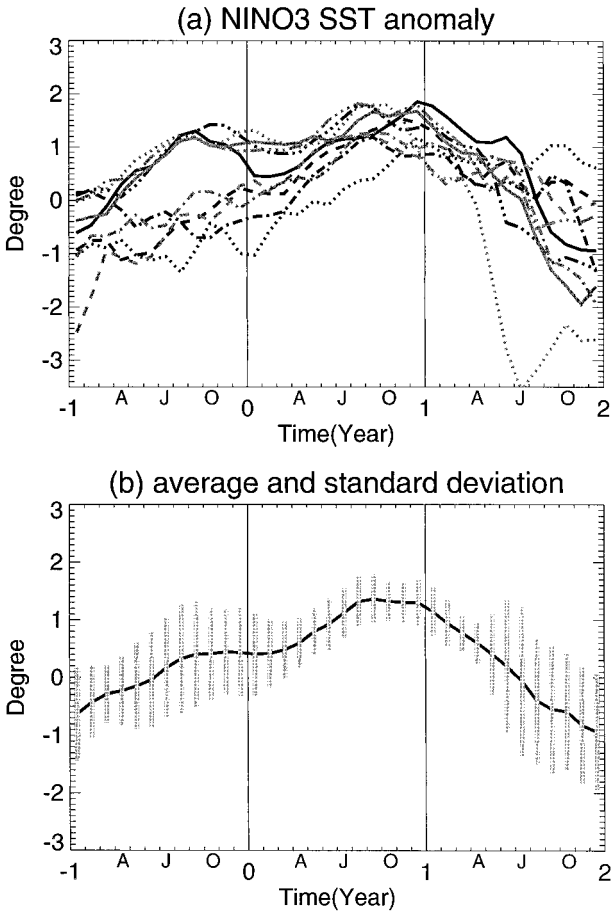

FIG. 10. As in Fig. 2, but with the atmospheric noise included. Ten El Niños are included.

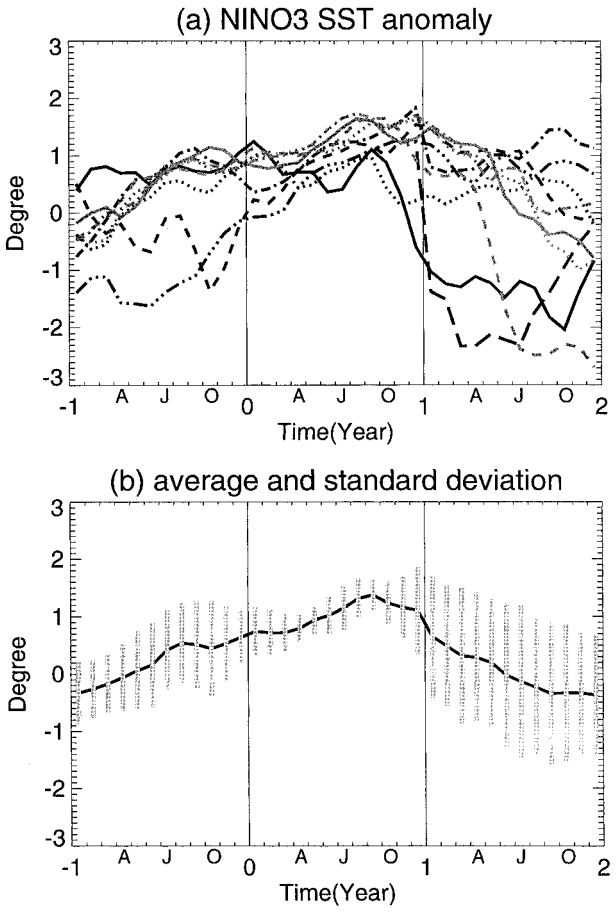

FIG. 11. As in Fig. 10, but for the case in Fig. 4c. Eight El Niños are included.

We suggest a link between the observed variations in onset and termination phases, and the scatter in these found in the models.

Atmospheric stochastic forcing (weather noise) is an obvious candidate for producing variations in phase locking. Weather noise has been shown to be important in many aspects of ENSO irregularity, as discussed in the introduction. However, it is of interest if there is also a deterministic mechanism that tends to produce scatter in onset and termination of warm events, since this mechanism might have more favorable consequences for predictability. We therefore examine this phase-locking mechanism for producing scatter first in the deterministic case, and then we examine how it interacts with weather noise.

The phase-locking behavior in the model results can be explained as follows. ENSO cycles tend to peak in a preferred season, but with some adjustments resulting from the integrated effects from the duration of past events. In this mechanism, there are two competing effects: (i) the inherent ENSO frequency (the frequency in absence of the annual cycle), which is not phase locked if it does not have an integer-year period; and (ii) the nonlinear interaction of the ENSO cycle with the annual cycle, which tends to frequency-lock the ENSO cycle. In the simplest case, the frequency is nonlinearly adjusted so that the phase matches the favorable season for each event. This occurs in some of the cases where the inherent frequency is such that it is relatively easy to match an integer year. In many cases, there is a compromise between the preferred season for warming and the inherent length of the cycle, resulting in the ENSO warm phase not being perfectly locked to the preferred season but scattered around it.

Figure 14 schematizes this mechanism in an idealized case, in which the inherent ENSO period is close to 2.5 yr. This case with short ENSO period is chosen since it is easier to illustrate, but the principle extends to other inherent periods. In the schematic we also neglect amplitude variation, to focus on how nonlinear interaction with the seasonal cycle modifies the length of each ENSO cycle. Thick bars in the latter part of each calendar year indicate the favored season for maximum warming of the equatorial SST anomaly. We note that the seasonally dependent factors that lead to a preferred season for warming do not necessarily occur during this

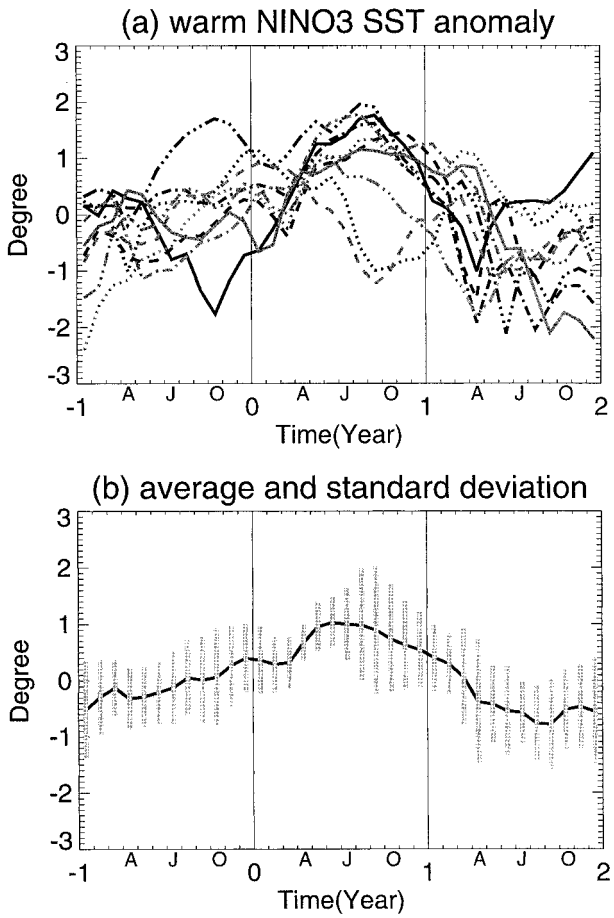

FIG. 12. As in Fig. 10, but for the case in Fig. 4d. Ten El Niños are included.

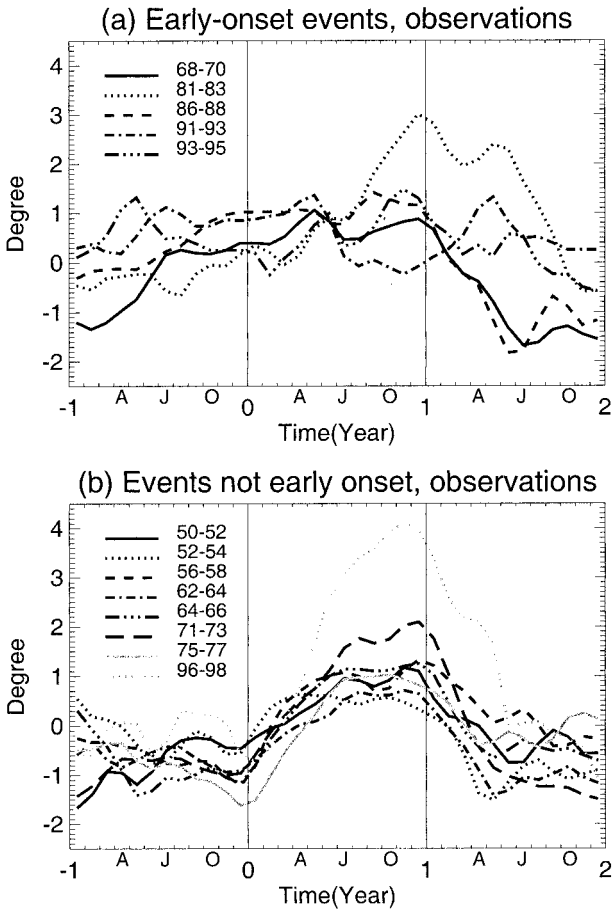

FIG. 13. Niño-3 indices of SST anomaly for observed El Niños categorized according to the onset index: (a) greater (early onset) and (b) smaller than the mean onset index. The onset index is defined as the 3-month mean of the SST anomaly centered at 12 months prior to the averaged peak month of the 13 observed warm events.

season, since the warming depends on tendencies integrated over previous seasons. The discussion is phrased in terms of a ''favored season'' for simplicity. The cycle is shown with the initial warm phase aligned with the favored season. The inherent period would lead to the next warm phase occurring slightly after the favored season. The seasonal factors that favor warming in the preferred season thus tend to shorten the first cycle so the warming occurs earlier, closer to the preferred season. Memory of the preferred length of the cycle is preserved in other parts of the system, so the second cycle tends to be stretched, and the seasonal factors tend to stretch it to 3 yr so it can also occur in the preferred season. The averaged cycle length is close to the inherent period but a rational multiple (5/2) of a year. When the warm phases of these two cycles are compared, using the format with the maximum SST anomaly aligned in the central year of a 3-yr interval (lower panel of Fig. 14), scatter is seen in the onset. The cycle that is stretched has a more gradual warming that begins earlier, compared to the cycle whose duration has been shrunk. In this case with a simple alternation of 2- and 3-yr cycle lengths, there are only two onset patterns, which repeat. More complicated onset (or termination) behavior is possible for other frequency-locking sequences, which would occur for other values of the inherent period.

Phase locking can be very sensitive to parameters even when the locked frequency is unchanged. The simple-model results show, for instance, that by slightly varying the coupling coefficient, the warm-peak phase can be shifted from summer to winter season while the frequency is still locked to the same frequency step. Similar sensitivity is seen in the HCM. This difference between phase-locking and frequency-locking behavior is illustrated in Fig. 15. Frequency-locked solutions are shown as a function of the inherent ENSO frequency, which can be controlled in a model by varying any of several parameters. The frequency ratio of ENSO to the annual cycle remains constant over an interval and then changes in a discrete jump to the next frequency-locked solution (e.g., Jin et al. 1994, 1996; Tziperman et al. 1994; chaotic regimes are omitted for clarity). The behavior of the phase of the ENSO cycle relative to the

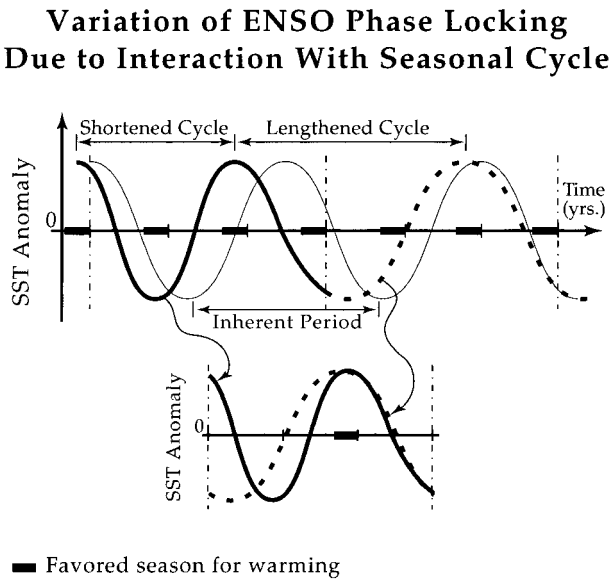

FIG. 14. Schematic of the mechanism of ENSO phase variation by frequency locking. The inherent ENSO cycle (thin solid line) that would occur in absence of the seasonal cycle is shown for a case with period slightly longer than 2.5 yr. The length of the ENSO cycle is modified by nonlinear interaction so that warming tends to occur in the favored season (indicated by thick bars). In this example, this produces an alternation of approximately 2-yr (thick solid curve) and 3-yr (dashed solid curve) ENSO cycles. Displaying these (lower panel) in the format of Fig. 1, the evolution of the onset of the warming differs, despite the overall simplicity of the cycle.

annual cycle can change considerably over one of these parameter intervals, even though the frequency ratio is constant. The case shown here is relatively simple in that there is a unique month in which the maximum warming occurs for all events. Even in this simple case, the ENSO phase relation to the seasonal cycle can vary considerably over a small parameter interval. Current theory seems to provide no means of distinguishing conditions under which the seasonal phasing of ENSO is robust from conditions that have a subtle parameter dependence such as illustrated here.

The effect of weather noise on this mechanism is also examined. A stochastic process independent of season is used, so it is clear that all seasonal aspects of the behavior arise from the deterministic part of the system. In cases where the phase locking is complicated in the deterministic case, similar results for onset and termination phases are seen in presence of noise. Weather noise makes the biggest difference in cases where the deterministic behavior is particularly simple, essentially by making the scatter in onset and termination phases look like the more complicated cases. The potential impact of seasonal dependence in the weather noise is hard to assess quantitatively. However, we note that quite complex, and in some respects realistic, phase-locking behavior can be obtained just with the deterministic phase-locking mechanism plus season-independent noise.

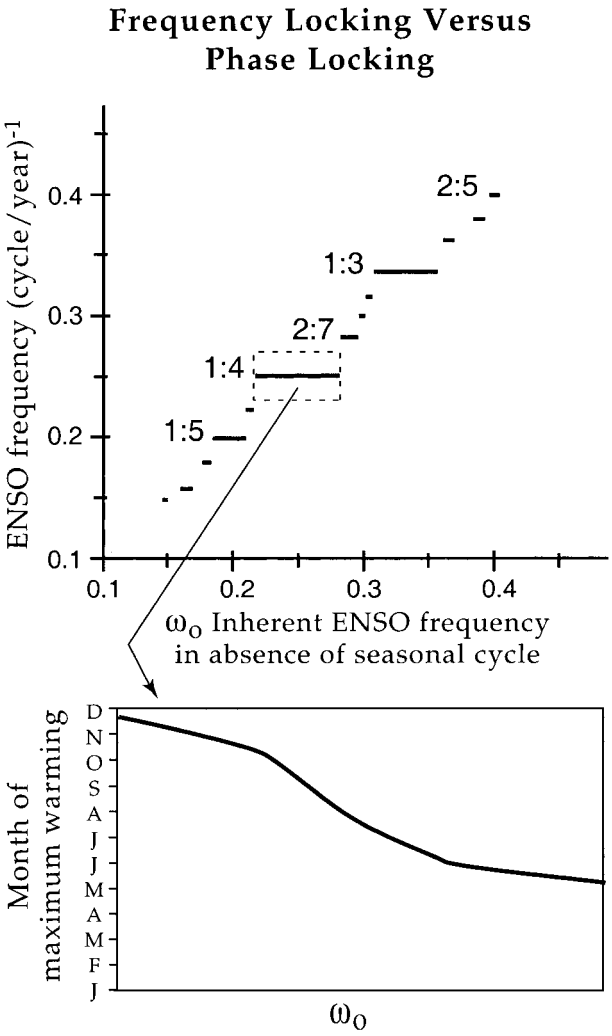

FIG. 15. Schematic of the difference between phase-locking and frequency-locking behavior. The frequency ratio of the number of ENSO cycles per annual cycle (or the dominant ENSO frequency in cycles per year) is shown as a function of the inherent ENSO frequency (which summarizes the effects of external parameters). The frequency ratio changes in a sequence of frequency-locked discrete ''steps.'' The lower panel shows a measure of the phase-locking behavior, the month of maximum warming, over one of these steps. Even though the frequency locking is constant over the interval, the phase-locking behavior changes. In the models it can show considerable variation within a small parameter range.

Motivated by the mechanism for the variations in model phase-locking behavior, we analyzed the variations in observed El Niño events. An interesting case occurs when we define a category for early-onset El Niños. The early-onset El Niños appear to behave differently from the rest, with broad warm phases and more irregular behavior. We conjecture that since the early onset El Niños do not have a suitable season to start with, nonlinearity would have to work harder to force the peak phase toward the preferred season. With either a stronger role of nonlinearity or the maximum occurring at a different season, the early-onset El Niños show

more irregular behavior and may thus be more difficult to predict.

While frequency locking has been studied in many nonlinear systems (Iooss and Joseph 1990), we note that the study of phase locking in these ENSO systems has some interesting behavior that adds additional aspects to the frequency locking. The sensitivity of the maximum warming season to parameters even for a given frequency locking, and the scatter of onset and termination phases, provide examples of this. In summary, we argue that the notion of a sharply preferred season for observed El Niños appears to be an oversimplification. Taking variations of ENSO phase locking in model results as a prototype, we suggest that the observed scattered behavior of onset and termination phases is a fundamental ENSO property.

Acknowledgments. This work was supported in part by National Oceanic and Atmosphic Administration (NOAA) Grants NA56GP0451 and NA86GP0314 (HHS and JDN) and NAGC95773 (FFJ) and National Science Foundation (NSF) Grant ATM-9521389 (HHS and JDN) and ATM-9615952 (FFJ). Computations were carried out at the National Center for Atmospheric Research, which is sponsored by NSF, and at The Florida State University Computer Center, sponsored by the NOAA Climate and Global Change Program. We thank Dr. Lee-Lueng Fu at the California Institute of Technology Jet Propulsion Laboratory (JPL) for supporting HHS in finishing this paper at JPL. A visit by FFJ to UCLA was partially supported by JIMAR of University of Hawaii and UCLA IGPP.

APPENDIX

The Impact of Atmospheric Adjustment Timescale on Frequency of Coupled Mode

In both Syu and Neelin (2000a,b) and this paper, we include an adjustment time in the atmospheric model. Although it is relatively small compared to ENSO timescales, it can affect the ENSO period. Since it is relatively easy to adjust without impacting the climatology, this atmospheric adjustment time is varied in many of the experiments used here. We thus include a brief analysis of the variation between this parameter and the change of the ENSO period. For a slaved atmospheric model, the relation between wind stress and SST anomaly can be simply written as

$$\tau' = \mu\mathcal{A}(T'), \tag{A1}$$

where $\mathcal{A}$ is a linear operator and μ is the relative coupling coefficient. Now let us assume that the atmosphere actually has an adjustment timescale, and it takes some time for the atmosphere to reach the equilibrium response described in (A1). The adjustment processes can be written as

$$\frac{d}{dt}T'_{\text{adj}} = \frac{1}{\eta}(\tau' - \tau'_{\text{adj}}). \tag{A2}$$

In other words, atmosphere takes an e-folding time η to adjust to the quasi-steady response.

When $\mathcal{A}$ is linear, this is equivalent to defining

$$\frac{d}{dt}T'_{\text{adj}} = \frac{1}{\eta}(T' - T'_{\text{adj}}) \quad \text{and} \tag{A3}$$

$$\tau'_{\text{adj}} = \mu\mathcal{A}(T'_{\text{adj}}), \tag{A4}$$

where

$$T'_{\text{adj}} = \frac{1}{\eta}\int_0^t T'(t - s)e^{-s/\eta}\, ds \tag{A5}$$

is a weighted average of SST on the timescale of atmospheric adjustment and is identical to that in Syu and Neelin (2000a).

To elucidate the effect of the atmospheric adjustment on the eigenvalues of the coupled modes, we can consider a general eigenform of solution:

$$T' = Be^{\sigma t}. \tag{A6}$$

Here, σ is an eigenvalue of the coupled system. Then,

$$T'_{\text{adj}} = \frac{T'}{1 + \sigma\eta}. \tag{A7}$$

Or, in other words, when we take the effect of the atmospheric adjustment timescale into consideration, we get an effective coupling coefficient,

$$\mu_{\text{adj}} = \frac{\mu}{1 + \sigma\eta}. \tag{A8}$$

For different coupled modes, the correction factor $1/(1 + \sigma\eta)$ is different.

We are interested in the leading mode dominating the ENSO-like variability of the system. Assuming it follows the dispersion relation

$$\sigma = \sigma(\mu), \tag{A9}$$

then the correction on σ due to a finite η can be determined through a perturbation method if $|\sigma\eta| \ll 1$:

$$\sigma_{\text{adj}} - \sigma = \sigma(\mu_{\text{adj}}) - \sigma(\mu) \doteq \left.\frac{\partial\sigma}{\partial\mu}\right|_{\mu}(\mu_{\text{adj}} - \mu)$$

$$= \left.\frac{\partial\alpha}{\partial\mu}\right|_{\mu}\frac{\sigma\eta}{1 + \sigma\eta}\mu, \tag{A10}$$

where σ_{adj} denotes the eigenvalue including effects of atmospheric adjustment, with σ denoting the value when $\eta = 0$.

Consider a coupling coefficient near the critical value $\mu \simeq \mu_c$,

$$\left.\frac{\partial\sigma}{\partial\mu}\right|_{\mu_c} = a + ib. \tag{A11}$$

Normally, $a > 0$, when growth rate increases as μ increases, whereas b can be either positive or negative.

Thus,

$$\Delta\sigma = -(a + ib)\frac{\sigma\eta}{1 + \sigma\eta}\mu_c.$$

For $\sigma|_{\mu_c} \doteq i\omega_0$ and $\omega_0\eta \ll 1$, the frequency reduction is

$$\Delta\sigma_i = -\eta a\mu_c. \tag{A12}$$

In Syu and Neelin (2000a), we estimate $a\mu_c = 1/12$ months. Thus, one can estimate the periods of ENSO mode are 3, 3.33, 3.67, and 4 yr for $\eta = 0$, 1, 2, and 3 months, respectively. This is close to the numerical results of 3-, 3.35-, 3.71-, and 4.05-yr periods for $\eta = 0$, 1, 2, and 3 months. In the simple coupled model of the paper, we found $a\mu_c \simeq 1/6$ months. The ENSO periods are 3, 3.25, 3.25, 3.75, and 4 yr for $\eta = 0$, 10, 20, 30, and 42.5 days, respectively. These results are also consistent with the numerical solutions.

Normally, near the critical value of the coupling coefficient, *b* is smaller than *a*; therefore the growth rate correction is less significant. However, depending on the sensitivity of the growth rate of the ENSO mode on the coupling coefficient, the frequency of ENSO can be sensitive to the atmospheric adjustment timescale. Equation (A12) provides a good estimate of the frequency reduction due to the finite atmospheric adjustment timescale.

REFERENCES

Anderson, D. L. T., and J. P. McCreary, 1985: Slowly propagating disturbances in a coupled ocean–atmosphere model. *J. Atmos. Sci.,* **42,** 615–629.

Bak, P., 1986: The Devil's staircase. *Phys. Today,* **39**(12), 38–45.

Battisti, D. S., and A. C. Hirst, 1989: Interannual variability in a tropical atmosphere–ocean model: Influence of the basic state, ocean geometry and nonlinearity. *J. Atmos. Sci.,* **46,** 1687–1712.

——, and E. S. Sarachik, 1995: Understanding and predicting ENSO. *Rev. Geophys.,* (Suppl. B), **33**, 1367.

Blanke, B., J. D. Neelin, and D. Gutzler, 1997: Estimating the effects of stochastic wind stress forcing on ENSO irregularity. *J. Climate,* **10,** 1473–1486.

Cane, M. A., and S. E. Zebiak, 1985: A theory for El Niño and the Southern Oscillation. *Science,* **228,** 1084–1087.

——, M. Münnich, and S. E. Zebiak, 1990: A study of self-excited oscillations of the tropical ocean–atmosphere system. Part I: Linear analysis. *J. Atmos. Sci.,* **47,** 1562–1577.

Chang, P., B. Wang, T. Li, and L. Ji, 1994: Interactions between the seasonal cycle and the Southern Oscillation—Frequency entrainment and chaos in an intermediate coupled ocean–atmosphere model. *Geophys. Res. Lett.,* **21,** 2817–2820.

——, L. Ji, B. Wang, and T. Li, 1995: Interactions between the seasonal cycle and El Niño–Southern Oscillation in an intermediate coupled ocean–atmosphere model. *J. Atmos. Sci.,* **52,** 2353–2372.

——, ——, H. Li, and M. Flügel, 1996: Chaotic dynamics versus stochastic processed in El Niño–Southern Oscillation in coupled ocean–atmosphere models. *Physica D,* **98,** 301–320.

——, ——, and ——, 1997: A decadal climate variation in the tropical Atlantic Ocean from thermodynamic air–sea interactions. *Nature,* **385,** 516–518.

Cox, M. D., 1984: A primitive equation, 3-dimensional model of the ocean. GFDL Ocean Group Tech. Rep. 1, NOAA/GFDL, Princeton, NJ.

Deser, C., and J. M. Wallace, 1990: Large-scale atmospheric circulation features of warm and cold episodes in the tropical Pacific. *J. Climate,* **3,** 1254–1281.

——, M. A. Alexander, and M. S. Timlin, 1996: Upper-ocean thermal variations in the North Pacific during 1970–1991. *J. Climate,* **9,** 1840–1855.

Eckert, C., and M. Latif, 1997: Predictability of a stochastically forced hybrid coupled model of El Niño. *J. Climate,* **10,** 1488–1504.

Gu, D., and S. G. H. Philander, 1997: Interdecadal climate fluctuations that depend on exchanges between the tropics and extratropics. *Science,* **275,** 805–807.

Horel, J. D., 1982: The annual cycle in the tropical Pacific atmosphere and ocean. *Mon. Wea. Rev.,* **110,** 1863–1878.

Iooss, G., and D. D. Joseph, 1990: *Elementary Stability and Bifurcation Theory.* Springer-Verlag, 324 pp.

Jensen, M. H., P. Bak, and T. Bohr, 1984: Transition to chaos by interaction of resonances in dissipative systems. Part I. Circle maps. *Phys. Rev. A,* **30,** 1960–1969.

Jin, F.-F., 1996: Tropical ocean-atmosphere interaction, the Pacific cold tongue, and the El Niño–Southern Oscillation. *Science,* **274,** 76–78.

——, 1997a: An equatorial recharge paradigm for ENSO. Part I: Conceptual model. *J. Atmos. Sci.,* **54,** 811–829.

——, 1997b: An equatorial recharge paradigm for ENSO. Part II: A stripped-down coupled model. *J. Atmos. Sci.,* **54,** 830–845.

——, and J. D. Neelin, 1993a: Modes of interannual tropical ocean–atmosphere interaction—A unified view. Part I: Numerical results. *J. Atmos. Sci.,* **50,** 3477–3503.

——, and ——, 1993b: Modes of interannual tropical ocean–atmosphere interaction—A unified view. Part III: Analytical results in fully coupled cases. *J. Atmos. Sci.,* **50,** 3523–3540.

——, ——, and M. Ghil, 1994: El Niño on the devil's staircase: Annual subharmonic steps to chaos. *Science,* **264,** 70–72.

——, ——, and ——, 1996. El Niño/Southern Oscillation and the annual cycle: Subharmonic frequency locking and aperiodicity. *Physica D,* **98,** 442–465.

Kleeman, R., and S. B. Power, 1994: Limits to predictability in a coupled ocean–atmosphere model due to atmospheric noise. *Tellus,* **46A,** 529–540.

——, and A. M. Moore, 1997: A theory for the limitation of ENSO predictability due to stochastic atmospheric transients. *J. Atmos. Sci.,* **54,** 753–767.

Latif, M., 1998: Dynamics of interdecadal variability in coupled ocean–atmosphere models. *J. Climate,* **11,** 602–624.

——, A. Sterl, E. Maier-Reimer, and M. M. Junge, 1993: Climate variability in a coupled GCM. Part I: The tropical Pacific. *J. Climate,* **6,** 5–21.

——, T. Stockdale, J. Wolff, G. Burgers, E. Maier-Reimer, M. M. Junge, K. Arpe, and L. Bengtsson, 1994: Climatology and variability in the ECHO coupled GCM. *Tellus,* **46A,** 351–366.

Legler, D. M., and J. J. O'Brien, 1984: Atlas of tropical Pacific wind stress climatology 1971–1980. Dept. of Meteorology, The Florida State University, Tallahassee, FL, 182 pp.

Liu, Z., S. G. H. Philander, and R. C. Pacanowski, 1994: A GCM study of tropical–subtropical upper-ocean water exchange. *J. Phys. Oceanogr.,* **24,** 2606–2623.

Münnich, M., M. A. Cane, and S. E. Zebiak, 1991: A study of self-excited oscillations in a tropical ocean–atmosphere system. Part II: Nonlinear cases. *J. Atmos. Sci.,* **48,** 1238–1248.

Neelin, J. D., 1991: The slow sea surface temperature mode and the fast-wave limit: Analytic theory for tropical interannual oscillations and experiments in a hybrid coupled model. *J. Atmos. Sci.,* **48,** 584–606.

——, and F.-F. Jin, 1993: Modes of interannual tropical ocean–atmosphere interaction—A unified view. Part II: Analytical results in the weak coupling limit. *J. Atmos. Sci.,* **50,** 3504–3522.

——, M. Latif, and F.-F. Jin, 1994: Dynamics of coupled ocean–

atmosphere models: The tropical problem. *Annu. Rev. Fluid Mech.,* **26,** 617–659.

——, D. S. Battisti, A. C. Hirst, F.-F. Jin, Y. Wakata, T. Yamagata, and S. E. Zebiak, 1998: ENSO theory. *J. Geophys. Res.,* **103,** 14 261–14 290.

Pacanowski, R. C., and S. G. H. Philander, 1981: Parameterization of vertical mixing in numerical models of the tropical oceans. *J. Phys. Oceanogr.,* **11,** 1443–1451.

Penland, C., and P. D. Sardeshmukh, 1995: The optimal growth of tropical sea surface temperature anomalies. *J. Climate,* **8,** 1999–2024.

Philander, S. G. H., T. Yamagata, and R. C. Pacanowski, 1984: Unstable air–sea interactions in the Tropics. *J. Atmos. Sci.,* **41,** 604–613.

Rasmusson, E. M., and T. H. Carpenter, 1982: Variations in tropical sea surface temperature and surface wind fields associated with the Southern Oscillation/El Niño. *Mon. Wea. Rev.,* **110,** 354–384.

Reynolds, R. W., 1988: A real-time global sea surface temperature analysis. *J. Climate,* **1,** 75–86.

——, and T. M. Smith, 1994: Improved global sea surface temperature analyses using optimum interpolation. *J. Climate,* **7,** 929–948.

Schopf, P. S., and M. J. Suarez, 1988: Vacillations in a coupled ocean–atmosphere model. *J. Atmos. Sci.,* **45,** 549–566.

Syu, H.-H., and J. D. Neelin, 2000a: ENSO in a hybrid coupled model. Part I: Sensitivity to physical parameterizations. *Climate Dyn.,* **16,** 19–34.

——, and ——, 2000b: ENSO in a hybrid coupled model. Part II: Prediction with piggyback data assimilation. *Climate Dyn.,* **16,** 35–48.

——,——, and D. Gutzler, 1995: Seasonal and interannual variability in a hybrid coupled GCM. *J. Climate,* **8,** 2121–2143.

Tziperman, E., L. Stone, M. Cane, and H. Jarosh, 1994: El Niño chaos: Overlapping of resonances between the seasonal cycle and the Pacific ocean–atmosphere oscillator. *Science,* **264,** 72–74.

——, M. A. Cane, and S. Zebiak, 1995: Irregularity and locking to the seasonal cycle in an ENSO prediction model as explained by the quasi-periodicity route to chaos. *J. Atmos. Sci.,* **52,** 293–306.

——, S. E. Zebiak, and M. A. Cane, 1997: Mechanisms of seasonal–ENSO interaction. *J. Atmos. Sci.,* **54,** 61–71.

——, M. A. Cane, S. E. Zebiak, Y. Xue, and B. Blumenthal, 1998: Locking of El Niño's peak time to the end of the calendar year in the delayed oscillator picture of ENSO. *J. Climate,* **11,** 2191–2199.

Wakata, Y., and E. S. Sarachik, 1991: Unstable coupled atmosphere–ocean basin modes in the presence of a spatially varying basic state. *J. Atmos. Sci.,* **48,** 2060–2077.

Waliser, D. E., B. Blanke, J. D. Neelin, and C. Gautier, 1994: Shortwave feedbacks and El Niño–Southern Oscillation: Forced ocean and coupled ocean–atmosphere experiments. *J. Geophys. Res.,* **99** (C12), 25 109–25 125.

Wallace, J. M., T. P. Mitchell, E. M. Rasmusson, V. E. Kousky, E. S. Sarachik, and H. von Storch, 1998: On the structure and evolution of ENSO-related climate variability in the tropical Pacific: Lessons from TOGA. *J. Geophys. Res.,* **103,** 14 241–14 260.

Wyrtki, K., 1986: Water displacements in the Pacific and the genesis of El Niño cycles. *J. Geophys. Res.,* **91,** 7129–7132.

Xie, S.-P., 1995: Interaction between the annual and interannual variations in the equatorial Pacific. *J. Phys. Oceanogr.,* **25,** 1930–1941.

Zebiak, S. E., 1989: On the 30–60-day oscillation and the prediction of El Niño. *J. Climate,* **2,** 1381–1387.

——, and M. A. Cane, 1987: A model El Niño–Southern Oscillation. *Mon. Wea. Rev.,* **115,** 2262–2278.